Computational Materials Science 47 (2009) 168–177

Contents lists available at ScienceDirect

Computational Materials Science

journal homepage: www.elsevier.com/locate/commatsci

Vibration analysis of multi-walled carbon nanotubes using a spring–mass based finite element model

S.K. Georgantzinos, N.K. Anifantis *

Machine Design Laboratory, Mechanical and Aeronautics Engineering Department, University of Patras, GR 26500, Greece

ARTICLE INFO

Article history:
Received 28 April 2009
Received in revised form 30 June 2009
Accepted 8 July 2009
Available online 12 August 2009

Keywords:
Multi-walled carbon nanotubes
Vibration analysis
Nanosprings
Finite element analysis

ABSTRACT

We report a study of the vibrational characteristics of multi-walled carbon nanotubes modeled exclusively using springs and lumped masses. Based on the atomic microstructure of the nanotube, three-dimensional nanoscale spring elements are utilized to simulate the dynamic behavior of each layer of the multi-walled carbon nanotubes. Appropriate spring elements are also developed to model the inter-layer interactions and describe the van der Waals potentials between carbon atoms on different layers. Direct application of the physical variables of molecular mechanics theory to the springs is used to simulate the relative translations and rotations between atoms as well as the masses of the carbon atoms. The stiffness and mass matrices of the problem are used to construct the dynamic equilibrium equation. The natural modes of vibration and the corresponding natural frequencies are derived by solving the eigenvalue problem for different support conditions. The present method suggests novel basic modes of vibration, beyond those reported in the literature pertaining to multi-walled carbon nanotubes. The effects on the basic modes and natural frequencies created by van der Waals interactions and geometric parameters such as number of layers and aspect ratio are investigated in the context of elastic support conditions. Comparisons with other theoretical studies reveal very good correlations in terms of fundamental modes and frequencies.

© 2009 Elsevier B.V. All rights reserved.

1. Introduction

Carbon nanotubes (CNTs) are molecular-scale tubes of graphite carbon and are among the most promising nanoscale components for nanostructures, nanodevices, nanocomposites, and various applications due to their exceptional physical and mechanical properties. This fact has attracted the interest of researchers in the development of theoretical models and experimental measurements used to predict the behavior of CNTs and to investigate their potential for novel applications. CNTs are the stiffest and strongest known fibers, with remarkable electronic properties and many other unique characteristics. For more detail on theoretical predictions and experimental measurements of both mechanical and physical properties, see the comprehensive reviews in [1,2].

The combination of an extremely high stiffness and light weight in CNTs results in vibration frequencies on the order of GHz and THz. The vibrational behavior of CNTs is a fundamental characteristic that should be fully studied because it is essential for applications such as electromechanical resonators, vibration sensors, charge detectors, and field emission devices. An excellent review article was recently published by Gibson et al. [3] that presents related scientific efforts in dealing with the vibrational behavior of CNTs and their composites, including both theoretical and experimental studies. Comparisons between experimental and theoretical methods beyond the geometric characteristics of the CNTs first require the complete definition of all parameters that influence the vibrational behavior, such as the slack phenomenon, the nature of support conditions, environmental conditions, and other factors. Garcia-Sanchez et al. [4] have recently presented a mechanical method for detecting CNT resonator vibrations using a novel scanning force microscopy method.

Because controlled experiments performed at nanoscale dimensions remain both difficult and expensive, theoretical methods such as molecular dynamics (MD) and molecular mechanics, as well as elastic continuum mechanics, are considered efficient because they can accurately and cost-effectively produce results that closely approximate the behavior of CNTs. Each of the previously mentioned approaches offers different advantages, but also certain drawbacks. MD is an accurate method capable of simulating the full mechanical CNT performance. However, it carries a high computational cost that may be prohibitive for large-scale problems, especially in the context of vibration analysis. Molecular mechanics-based techniques, such as those in [5–7], have been used for vibration analysis of CNTs and have been shown to be accurate and also more computationally cost-effective than MD. Nevertheless, under such approaches, the modeling of atomic interactions requires special attention because the mechanical equivalent used

* Corresponding author. Tel.: +30 2610 997 195; fax: +30 2610 997 207.
E-mail address: nanif@mech.upatras.gr (N.K. Anifantis).

0927-0256/$ - see front matter © 2009 Elsevier B.V. All rights reserved.
doi:10.1016/j.commatsci.2009.07.006

to simulate the carbon–carbon bond deformations must be efficient for the studied problem. An efficient mechanics-based numerical model [8] for the vibrational analysis of single-walled CNTs (SWCNTs) was recently published. The results of this study showed new basic vibrational modes of CNTs that had not been reported by other methods and also described the effects of defects on the natural frequencies. Kwon et al. [9] estimated the natural frequencies and mode shapes of various carbon nanotubes using eigenvalue analysis of mass and stiffness matrices directly computed from atomistic simulations. In contrast, elastic continuum mechanics methods based on well-known beam theories have also been successfully used to evaluate the vibration characteristics of CNTs under typical boundary conditions [10–13]. Xu et al. [14] studied the free vibration of double-walled CNTs modeled as two individual beams interacting with each other taking van der Waals forces into account and supported with different boundary conditions between the inner and outer tubes. These methods have the lowest computational cost; however, they can compute only a subset (mainly the bending modes) of the vibrational modes and natural frequencies.

In this paper, we study the vibrational characteristics of multi-walled CNTs (MWCNTs). The method uses spring–mass elements that simulate the interatomic interactions and the mass effects in every layer of the MWCNTs. It uses a special technique for simulating the bending between adjacent bonds, distinguishing it from other mechanics-based methods. This method utilizes the exact microstructure of the CNTs while allowing the straightforward input of the force constants that molecular theory provides. In addition, spring-like elements are formulated in order to simulate the interlayer van der Waals interactions. These elements connect all atoms between different layers at a distance smaller than the limit below which the van der Waals potential becomes zero. The related stiffness is a function of this distance. We use modeling considerations that are entirely compatible with molecular theory and are not presented elsewhere for the vibrational analysis of MWCNTs. The resulting dynamic equilibrium equations can be used to generate new results. By applying different support conditions, comparisons with fundamental frequencies as suggested by other methods (where possible) demonstrate remarkable agreement. To our knowledge, there has been no complete study of vibrational characteristics of MWCNTs with respect to all relevant geometric nanotube parameters. Here, we present a parametric analysis and we report the natural frequencies as well as the mode shapes of various MWCNTs for different aspect ratios and numbers of layers. Moreover, we also investigate the effect of elastic support conditions on the natural frequencies, another area that has not been studied to date. Our method reveals new mode shapes that in several cases are basic and have not yet been reported in the literature.

2. MWCNT geometric specifications

Numerous articles report the main geometric characteristics of nanotubes. A multi-walled carbon nanotube consists of multiple layers of graphite rolled to form a tube. In other words, a MWCNT consists of more than one coaxial SWCNT, where the interlayer distance is close to the distance between graphene layers in graphite, i.e., approximately 0.34 nm. Further detail on geometries can be found in [8,15].

The outer diameter D_{out} of a MWCNT can be calculated from the diameter of the corresponding outer (n, m) SWCNT as given by the following equation:

$$D_{out} = \frac{a_{c-c}\sqrt{3(n^2 + nm + m^2)}}{\pi}, \tag{1}$$

where the integers (n, m) express the number of steps along the zigzag carbon bonds [15] (and generally are used to name a nanotube) and a_{c-c} is the distance between two neighboring carbon atoms, equal to 0.1421 nm.Given that the interlayer distance is 0.34 nm (as observed in [16]), the difference between diameters of neighboring layers, where the diameter of every layer can be also calculated using Eq. (1), is $\Delta D = 0.68$ nm. Knowing that this equation is a function only of the chirality indices of the two neighboring nanotubes in a MWCNT, one can readily calculate the types of SWCNTs that are a part of the MWCNT with a specified number of layers and outer diameter. If (n_1, m_1) and (n_2, m_2) are the types of the inner and outer neighboring layers, respectively, we note that for zigzag nanotubes, the chirality indexes are $n_2 = n_1 + 9$ and $m_2 = m_1 = 0$. Correspondingly, if the neighboring nanotubes exhibit armchair configurations, then $n_2 = m_2 = n_1 + 5$ and $m_1 = n_1$. The type of MWCNT is declared in terms of the type sequences of all the layers $(n_{in}, m_{in}) - \ldots - (n_{out}, m_{out})$, starting from the type of the innermost tube and finishing with the type of the outermost tube. Therefore, the zigzag MWCNT that comprises ℓ layers can be specified as

$$(n_{out} - 9(\ell - 1), 0) - (n_{out} - 9(\ell - 2), 0) - \ldots - (n_{out} - 9, 0) - (n_{out}, 0), \tag{2}$$

where n_{out} is the n chirality index of the outermost layer, and the m chirality index for all the layers is equal to zero. The type of an armchair multi-walled nanotube consisting of ℓ number of layers is:

$$(n_{out} - 5(\ell - 1), n_{out} - 5(\ell - 1)) - (n_{out} - 5(\ell - 2), n_{out} - 5(\ell - 2)) - \ldots - (n_{out}, n_{out}), \tag{3}$$

and the n and m indices are equal to each other for every armchair layer.

Knowing the type of every layer and the length of the tube, the chiral vector and the translational vector that define the ideal rectangular cutting area of the graphene sheet are known [17]. Hence, the original coordinate system of the graphene sheet (x', y') is transformed into a new system (x, y, z) on the nanotube such that the translational vector lies along the y' -axis. Then, the graphene atomic coordinates are converted to those of the corresponding layer according to the equation (Kołoczek et al. [18])

$$(x, y, z) = \left(R\cos\left(\frac{x'}{R}\right),\ R\sin\left(\frac{x'}{R}\right),\ y'\right), \tag{4}$$

where R is the nanotube-layer radius.

All of the geometric characteristics, such as chirality angles and diameters, can be readily evaluated since they are dependent only on chiral indices. The overall length of every layer is the same as the length L of the MWCNT. A complete formula list for all parameters can been found in [17]. Consequently, the global design parameters of MWCNTs are the number of layers, the chiral indices of every layer, and the length of the tube.

3. Computational model

Our MWCNT modeling effort is based on linear nanosprings, as referred to in [8], which simulate the interatomic behavior. The hexagonal unit lattice of the CNT is simulated as a lattice of nanosprings. In order to accurately model the mass of the tube, specific masses are assumed to be concentrated at the nodes of particular nanosprings such that a total mass equal to the mass of the carbon nuclei is placed at each carbon position. Moreover, additional nanosprings are incorporated to simulate the required interlayer interactions.

3.1. Interatomic behavior modeling

In this work, we use the potential energy to evaluate nanospring stiffness. The total force on each atomic nuclei is the sum of the force generated by the electrons and the electrostatic force between the positively charged nuclei themselves. The general formula for the potential energy is

$$U = \sum U_r + \sum U_\theta + \sum U_\phi + \sum U_\omega + \sum U_{vdw}, \tag{5}$$

where U_r represents the energy due to bond stretching, U_θ the energy due to bond angle bending, U_φ the energy due to dihedral angle torsion, U_ω the energy due to out-of-plane torsion, and U_{vdw} the energy due to nonbonded van der Waals interactions.

Under the assumption of small deformations, the harmonic approximation is adequate for describing potential energy (Gelin [19]) and therefore characterizes the force field. By adopting the simplest harmonic forms and combining the dihedral angle torsion with the out-of-plane torsion into a single equivalent term, the following terms describe the total potential energy:

$$U_r = \frac{1}{2}k_r(\Delta r)^2, \quad \frac{d^2U_r}{d\Delta r^2} = k_r, \tag{6}$$

$$U_\theta = \frac{1}{2}k_\theta(\Delta\theta)^2, \quad \frac{d^2U_\theta}{d\Delta\theta^2} = k_\theta, \tag{7}$$

$$U_\tau = U_\phi + U_\omega = \frac{1}{2}k_\tau(\Delta\phi)^2, \quad \frac{d^2U_\tau}{d\Delta\tau^2} = k_\tau, \tag{8}$$

where k_r, k_θ, and k_τ are the bond stretching, bond angle bending, and torsional resistance force constants, respectively, while Δr, $\Delta\theta$, and $\Delta\phi$ represent the bond length, bond angle, and twisting bond angle variations. In contrast to the other bonded interactions, the van der Waals interactions and the electrostatic forces may be neglected due to their minor effects in terms of predicting the dynamic response of CNTs.

The second derivatives of the potential energy terms in Eqs. (6)–(8) with respect to bond length, bond angle and twisting bond angle variations produce the spring stiffness coefficients k_r, k_θ, and k_τ, according to Castigliano's theorem. These force field constants are consistent with the molecular mechanics, which can be straightforwardly introduced in nanosprings as spring stiffness constants. The angle bending interaction is simulated with an axial nanospring, using the simplification described in [15]. The stiffness k_b of the specific spring is described by the following equation:

$$k_b = \left(\frac{1}{a_{c-c}\cos(90^\circ - \gamma)}\right)^2 k_\theta, \tag{9}$$

where $\gamma = 30°$ in the hexagonal lattice of the graphene. This angle may vary for each C–C–C microstructure in a CNT according to its type and radius, due to its cylindrical shape. The spring stiffness coefficients of Eqs. (6)–(9) are taken to be equal to $k_r = 6.52 \times 10^{-7}$ N nm^{-1}, $k_\theta = 8.76 \times 10^{-10}$ N nm rad^{-2} (Cornell et al. [20]), and $k_\tau = 2.78 \times 10^{-10}$ N nm rad^{-2} (Cornell et al. [20] and Jorgensen and Severance [21]), respectively. In order to simulate the inertia effects, a point mass equal to a whole or half of the carbon atomic nucleus mass ($m = 1.9943 \times 10^{-26}$ kg) is added to one node in particular elements only. The masses of electrons are neglected. The analytical description of the spring–mass modeling of a CNT hexagonal lattice is reported in [8].

The interlayer interaction is described by the van der Waals potential. The Lenard–Jones 6–12 potential is utilized to express the interaction of carbon atoms located on different walls

$$U(R) = 4\varepsilon\left[\left(\frac{\sigma}{R}\right)^{12} - \left(\frac{\sigma}{R}\right)^{6}\right], \tag{10}$$

where R is the interatomic distance, and ε and σ are the Lenard-Jones parameters. For carbon atoms, the parameters are $\varepsilon = 3.8655 \times 10^{-13}$ N nm and $\sigma = 0.34$ nm, respectively [7]. Let R_1 be the initial distance between two carbon atoms located in different walls. We consider a nanospring with initial length R_1 in order to describe the van der Waals interaction. Consistent with the stiffness definition of the proposed nanospring, we define k_{vdw} as the stiffness coefficient, obtained from the second derivative of the van der Walls potential energy for distance R_1 as follows:

$$k_{vdw} = \frac{d^2U(R_1)}{dR_1^2} = 24\varepsilon\left(26\frac{\sigma^{12}}{R_1^{14}} - 7\frac{\sigma^6}{R_1^8}\right), \tag{11}$$

Given this van der Waals potential, we claim that when the distance R is larger than $2.5\sigma = 0.85$ nm, the effect of the van der Waals force can be neglected. Hence, van der Waals nanosprings are created for the pairs of atoms between different layers that exhibit distances smaller than 2.5σ.

3.2. Computer implementation

In order to evaluate the vibrational characteristics of MWCNTs, we must develop equations that describe the dynamic equilibrium of the entire model. The elemental equations must be constructed first before the global stiffness and mass matrices can be assembled.

The elemental equation for the a_i-element, as defined and developed in [8] to represent the bond stretching as well as twisting bond angle interactions, is

$$\begin{bmatrix} k_r\mathbf{I_{20}} & \mathbf{0} \\ \mathbf{0} & k_\tau\mathbf{I_{20}} \end{bmatrix}\begin{bmatrix} \mathbf{u} \\ \theta \end{bmatrix} + \begin{bmatrix} m_r\mathbf{I_{21}} & \mathbf{0} \\ \mathbf{0} & \mathbf{0} \end{bmatrix}\begin{bmatrix} \ddot{\mathbf{u}} \\ \ddot{\theta} \end{bmatrix} = \begin{bmatrix} \mathbf{F} \\ \mathbf{T} \end{bmatrix} \quad \text{or } \mathbf{k_a U} + \mathbf{m_a}\ddot{\mathbf{U}} = \mathbf{P}, \tag{12}$$

where

$$\mathbf{I_{20}} = \begin{bmatrix} 1 & -1 \\ -1 & 1 \end{bmatrix}, \quad \mathbf{I_{21}} = \begin{bmatrix} 0 & -1 \\ 0 & 1 \end{bmatrix}, \tag{13}$$

m_r is the concentrated mass equal to the half or whole mass of the carbon nuclei [8], $\mathbf{F}$ represents the forces applied to nodes 1 and 2 of the element, $\mathbf{u}$ is the vector of nodal displacements ($\mathbf{u} = [u_1 \quad u_2]^T$, $\mathbf{F} = [F_1 \quad F_2]^T$), $\boldsymbol{\theta}$ is the vector of nodal rotations, $\mathbf{T}$ is the vector of the applied torsional moments ($\theta = [\theta_1 \quad \theta_2]^T$, $\mathbf{T} = [T_1 \quad T_2]^T$), U is the vector of nodal translations and rotations, $\ddot{\mathbf{U}}$ is the vector of nodal accelerations, $\mathbf{P}$ is the column vector of loads, and finally, $\mathbf{k_a}$ and $\mathbf{m_a}$ are the elemental stiffness and mass matrix, respectively. Similarly, the equation for the b_i-element, which describes the bond angle interaction in the hexagonal lattice, is

$$\begin{bmatrix} k_b\mathbf{I_{20}} & \mathbf{0} \\ \mathbf{0} & \mathbf{0} \end{bmatrix}\begin{bmatrix} \mathbf{u} \\ \theta \end{bmatrix} + \begin{bmatrix} \mathbf{0} & \mathbf{0} \\ \mathbf{0} & \mathbf{0} \end{bmatrix}\begin{bmatrix} \ddot{\mathbf{u}} \\ \ddot{\theta} \end{bmatrix} = \begin{bmatrix} \mathbf{F} \\ \mathbf{T} \end{bmatrix} \quad \text{or } \mathbf{k_b U} + \mathbf{m_b}\ddot{\mathbf{U}} = \mathbf{P}, \tag{14}$$

where

$$k_b = \begin{cases} k_{b1}, & \text{when } b\text{-element is straight in respect to the hexagonal cell} \\ k_{b2}, & \text{when } b\text{-element is slant in respect to the hexagonal cell} \end{cases}$$

is the stiffness coefficient, as described in [15], and $\mathbf{k_b}$ and $\mathbf{m_b}$ are the corresponding elemental stiffness and mass matrix, respectively. Note that $\mathbf{m_b}$ is a null matrix.

Moreover, we must derive the elemental equation for the van der Waals nanosprings (*vdw* elements). Because this spring is only translational, we can write the elemental equation as follows:

$$\begin{bmatrix} k_{vdw}\mathbf{I_{20}} & \mathbf{0} \\ \mathbf{0} & \mathbf{0} \end{bmatrix} \begin{bmatrix} \mathbf{u} \\ \theta \end{bmatrix} + \begin{bmatrix} \mathbf{0} & \mathbf{0} \\ \mathbf{0} & \mathbf{0} \end{bmatrix} \begin{bmatrix} \ddot{\mathbf{u}} \\ \ddot{\theta} \end{bmatrix} = \begin{bmatrix} \mathbf{F} \\ \mathbf{T} \end{bmatrix} \quad \text{or} \quad \mathbf{k_{vdw}U} + \mathbf{m_{vdw}\ddot{U}} = \mathbf{P}, \tag{15}$$

where the mass matrix $\mathbf{m_{vdw}}$ is a null matrix. Here, it has to be noticed that the a_i-elements (Eq. (12)) include all the necessary inertia effects deriving from carbon atoms in a nanotube structure, while b_i and *vdw* elements (Eqs. (14) and (15), respectively) include only stiffness and no inertia terms (null mass matrices). According to the detailed description presented in [8], this technique ensures that a mass, which equals to carbon atomic nucleus, exists at every node – atom position after the assembly procedure.

Hence, the elemental matrices expressed in the global coordinate system are

$$\begin{aligned} \mathbf{K_a} &= \mathbf{T^T k_a T} \\ \mathbf{M_a} &= \mathbf{T^T m_a T} \\ \mathbf{K_b} &= \mathbf{T^T k_b T} \\ \mathbf{K_{vdw}} &= \mathbf{T^T k_{vdw}}, \end{aligned} \tag{16}$$

where $\mathbf{T}$ is the appropriate transformation matrix, as defined in [8]. The displacements and rotations as well as the loads are related by the equation

$$\mathbf{U} = \mathbf{TD}, \quad \mathbf{R} = \mathbf{T^T P}, \tag{17}$$

where $\mathbf{D}$ is the vector of displacements and rotations and $\mathbf{R}$ is the vector of loads with respect to the global coordinates. The superscript $\mathbf{T}$ in the above equations denotes matrix transposition. Finally, the elemental equations in the global system become

$$\mathbf{K_a D} + \mathbf{M_a \ddot{D}} = \mathbf{R}, \tag{18}$$

$$\mathbf{K_b D} + \mathbf{M_b \ddot{D}} = \mathbf{R}, \tag{19}$$

$$\mathbf{K_{vdw} D} + \mathbf{M_{vdw} \ddot{D}} = \mathbf{R}. \tag{20}$$

We assemble the global stiffness $\mathbf{K}$ and global mass matrices $\mathbf{M}$ from the above elemental matrices. Considering undamped free vibration for the tubes, the equation of motion becomes:

$$\mathbf{M\ddot{X}} + \mathbf{KX} = \mathbf{0}. \tag{21}$$

After applying the CNT support conditions, the eigenvalue problem can be solved using common finite element procedures. The solution to the eigenvalue problem reveals the natural frequencies of vibration and the corresponding mode shapes.

Fig. 1 shows an example of the proposed modeling technique. Fig. 1a shows the geometry of an armchair (3,3)-(8,8)-(13,13) MWCNT with length $L = 11$ nm. Fig. 1b depicts the corresponding model, which includes only those nanosprings that simulate the behavior of the individual layers. Due to the large number of *vdw* elements, they are best illustrated in cross-section (Fig. 1c). Table 1 presents information about some of the finite element meshes utilized in the analysis.

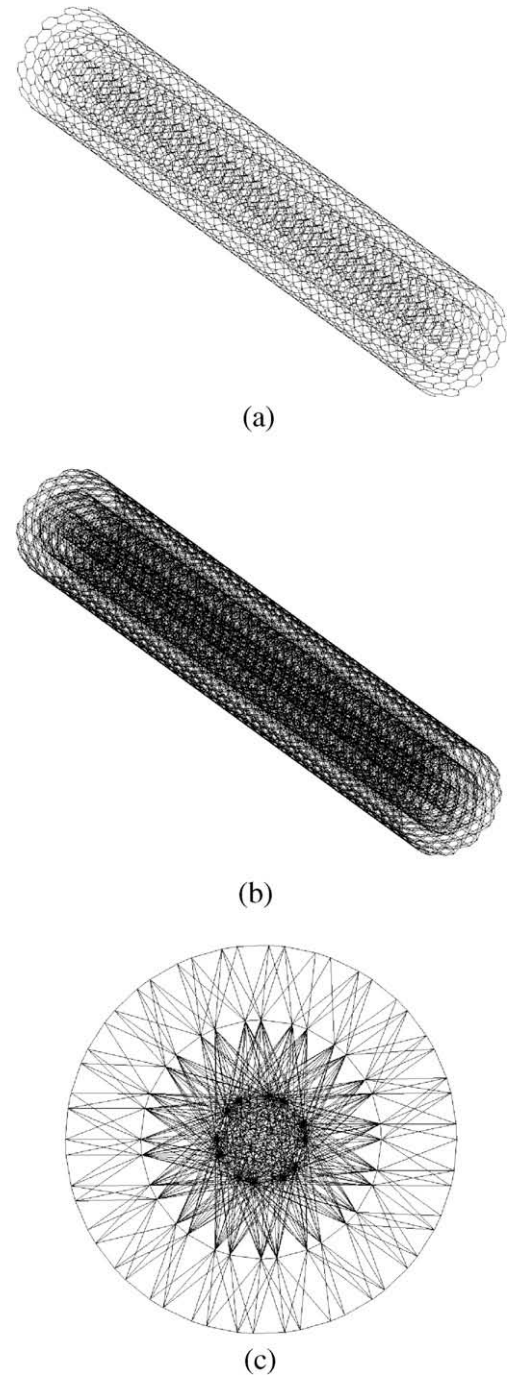

Fig. 1. MWCNT: (a) 3D geometry, (b) 3D model without *vdw* elements, and (c) model cross-section.

4. Results and discussion

First, in order to validate the proposed method, we compare the results obtained from the present method with outputs from other theoretical approaches based on molecular or continuum mechanics, as shown in Table 2. In the results of the studies [13,14], the nanotube type is not specified, obviously, because they are continuum approaches. In order to compare with them, we use zigzag (9,0)-(18,0) nanotubes presenting similar number of layers and dimensions (length and diameter). Further, the comparison is limited in terms of fundamental frequencies because the other methods obtain a different sequence of vibration modes. This is mainly because of differences in formulation as well as the presence of new modes that are not reported in the other methods. Very good agreement is shown between results for different support conditions.

First, we describe the shapes of the basic vibration modes for the usual clamped-free and clamped–clamped support conditions. Starting from the clamped–clamped case, Figs. 2 and 3 illustrate the modes of vibrations that may be basic depending on the geometric characteristics. The illustrated tube is an armchair (3,3)-(8,8)-(13,13) MWCNT with length $L = 11$ nm. Fig. 2 depicts modes that are important mainly for larger aspect ratios. Fig. 2a and b represents the first and second bending mode, where the tube shows a half-sine and full-sine shape, respectively, and behaves more like a beam. Fig. 2c illustrates the twisting (torsional) mode

Table 1
Finite element meshes used in our analysis.

Nanotube type	D_i (nm)	D_o (nm)	L (nm)	ℓ	Number of nodes	Number of *ai* elements	Number of *bi* elements	Number of *vdw* elements	Total number of elements
Armchair	0.4	1.8	11	3	4329	6432	12,768	220,413	239,613
	0.4	1.8	23	3	9024	13,488	26,880	467,703	508.071
	1.8	2.4	17	2	8618	12,865	25,606	312,138	350,609
	1.1	2.4	17	3	10,842	16,185	32,214	525,785	574,184
	0.4	2.4	17	4	11,676	17,430	34,692	821,415	885,213
Zigzag	0.4	1.8	12	3	4746	7056	13,505	234,249	254,810
	0.4	1.8	24	3	9492	14,154	27,178	544,930	586,262
	1.8	2.4	15	2	7755	11,550	23,045	271,643	306,238
	1.1	2.4	15	3	9729	14,490	28,911	455,966	499,367
	0.4	2.4	15	4	10,434	15,540	30,301	691,260	737,101

Table 2
Comparison of fundamental frequencies of MWCNTs resulting from different theoretical approaches*.

Nanotube type	D_i (nm)	D_o (nm)	L (nm)	Support condition of inner CNT	Support condition of outer CNT	Fundamental frequency (THz)	
						Present	Other studies
Zigzag	0.4	1.1	3.9	C–C	C–C	0.9410	0.9446 [7]
	0.4	1.1	5.6	C–C	C–C	0.5932	0.5774 [7]
	0.4	1.1	8.0	C–C	C–C	0.3467	0.3337 [7]
Armchair	0.4	1.1	4.1	C–C	C–C	0.9478	0.9276 [7]
	0.4	1.1	5.5	C–C	C–C	0.6410	0.7355 [7]
	0.4	1.1	8.0	C–C	C–C	0.3551	0.3323 [7]
Zigzag	0.7	1.4	14	Free	C–C	0.1582	0.1665 [14]
	0.7	1.4	14	Free	C–F	0.0288	0.0270 [14]
	0.7	1.4	14	C–C	C–C	0.1661	0.1718 [14]
Zigzag	0.7	1.4	20	C–C	C–C	0.04	~0.03 [13]

* Numbers in parentheses denote the corresponding reference.

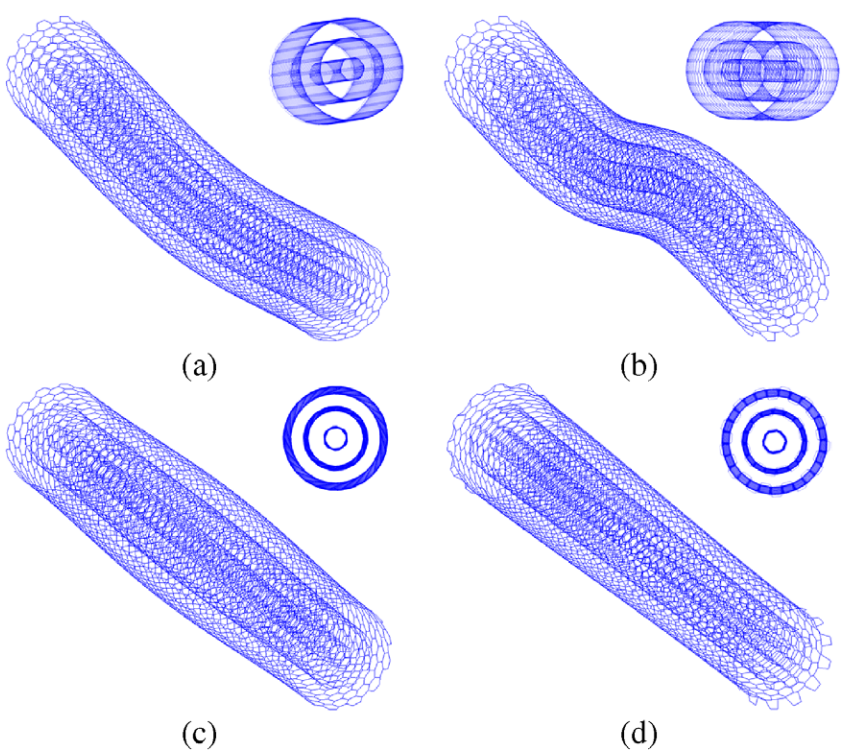

Fig. 2. Beam-like modes of vibration of clamped–clamped supported MWCNTs: (a) first bending, (b) second bending, (c) first twisting, and (d) first axial modes.

shape of vibration, in which the atoms move in the same circumferential direction with a simultaneous increase in the radius of every layer of the MWCNT. The maximum increase in the radius is observed on the half length of the tube. The first axial mode

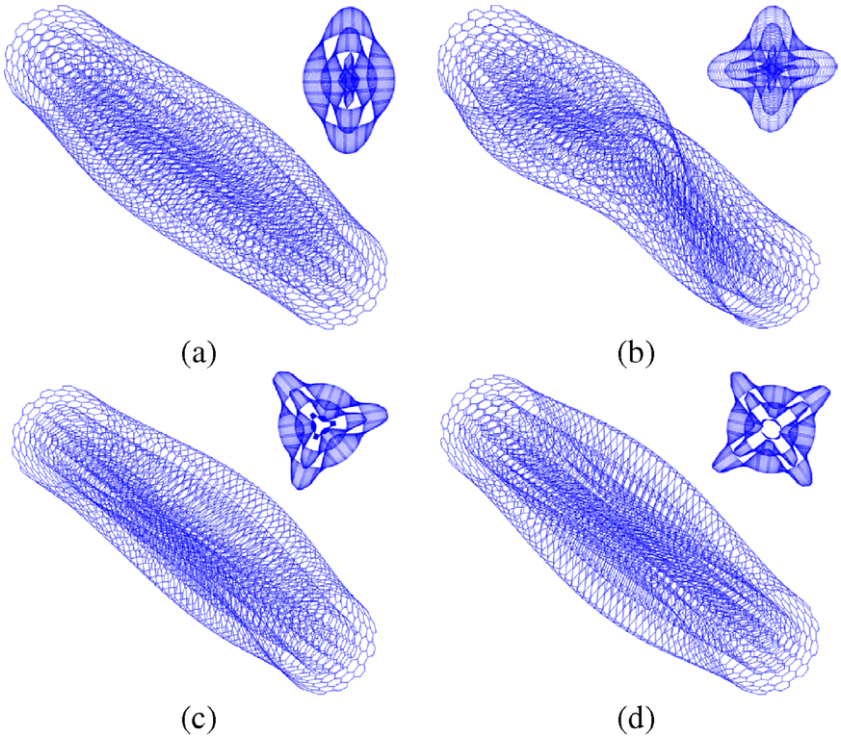

Fig. 3. Breathing modes of vibration of clamped–clamped supported MWCNTs: (a) first radial, (b) second radial, (c) first triangular, and (d) first cross modes.

(Fig. 2d) is accompanied by a simultaneous movement of all atoms in the longitudinal direction. In the second axial mode, we note longitudinal movement of the vectors towards the center of the tube. Fig. 3 depicts modes that are basic mainly for smaller aspect ratios. Fig. 3a and b represents the first and second radial breathing mode, respectively. In the first, the atoms at the half-length of the tube exhibit the greatest displacement due to the fixed-end boundary constraints. The second mode has a vase-like shape. Fig. 3c and d illustrates the first triangular and first cross mode shapes of vibration (this terminology is consistent with that used in [8] and refers to the corresponding modes of the SWCNT vibrations). These mode shapes are basic and sometimes fundamental. In the triangular mode, a triangle-like shape is observed at every cross-section of the tube, while in the cross mode, a cross shape is correspondingly observed at every cross-section. To the authors' best knowledge, this is the first time that these modes have been

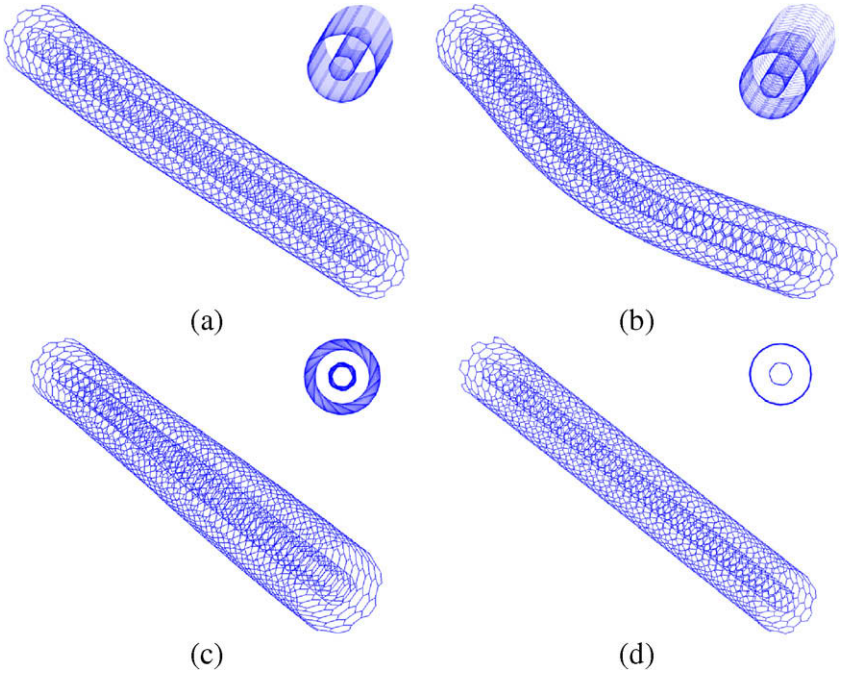

Fig. 4. Beam-like modes of vibration of clamped-free supported MWCNTs: (a) first bending, (b) second bending, (c) first twisting, and (d) first axial modes.

obtained and presented in the literature regarding MWCNT vibrations. We note the presence of mode shapes of vibration that differ from the conventional ones as seen in a beam of macro-scale dimensions.

For the clamped-free support condition, the basic mode shapes of vibration will be described for a zigzag (5,0)-(14,0) double-walled CNT with length $L = 15$ nm and using a much higher aspect ratio than the previous example. Fig. 4 correspondingly depicts modes that are basic for large aspect ratios. Fig. 4a and b illustrates the first and second bending mode shapes. These are similar to the bending modes presented in a macro-scale cantilever beam. The twisting modes (Fig. 4c) exhibit a behavior similar to the clamped–clamped case, but the shapes differ because of the free end. The first axial mode (Fig. 4d) is accompanied by a simultaneous movement of all atoms in the longitudinal direction and changing tube length during the vibration. In the cantilever case, there also exist breathing modes (Fig. 5). Some of these are deformed mainly at the free end. Depending on the circumstances, the free end takes on elliptical (Fig. 5a, first radial breathing mode), triangular-like (Fig. 5c, first triangular mode), cross-like (Fig. 5d, first cross mode), or more complicated shapes for higher frequencies. Fig. 5b illustrates the second radial breathing mode, which can also be basic. The second triangular and cross modes present similar behavior to the second radial mode; however, they exhibit triangular-like and cross-like cross-sections, in contrast to the elliptical shape of the radial breathing mode.

The next set of results refers to the natural vibrational frequencies ($f = \omega/2\pi$) of the MWCNTs. In Fig. 6, the effect of aspect ratio on an armchair (3,3)-(8,8)-(13,13) CNT is shown. Fig. 6a illustrates the behavior of major natural frequencies for different lengths and for the clamped–clamped support condition. We note that the greater the length, the lower the bending, axial, and twisting (torsional) natural frequencies. The radial type modes (i.e., the first radial as well as the cross and triangular modes) reach an almost constant value beyond a limiting length size. Hence, for large lengths, the first bending, first axial, and first twisting frequencies are lower than the radial ones. Consequently, the nanotube behaves like a beam. For small lengths, the breathing (radial, triangular, and cross) modes became basic. Fig. 6b illustrates similar frequency variations for the clamped-free support condition. Here, the nanotube is a zigzag (5,0)-(14,0)-(23,0) MWCNT.

In order to investigate the influence of the number of layers on the vibration characteristics of a nanotube, CNTs of the same aspect ratio (i.e., the same length and outer diameter) were chosen for analysis with the proposed technique. Fig. 7a depicts how the natural frequencies change for armchair tubes of length $L = 17$ nm and outer diameter $D_o = 2.45$ nm when subjected to a clamped–clamped support condition. It is observed that the lower the number of layers, the lower the frequency of the first radial breathing, second radial breathing, first triangular, and first cross modes. In contrast, the higher the number of layers, the lower the frequency of the first bending, second bending, first twisting, and first axial modes. As the number of layers increases, the tube tends to behave more like a beam. Note that for tubes with only one layer (SWCNTs), the basic modes are the first triangular, the first cross, and the first radial breathing shapes. Fig. 7b illustrates similar variations for the clamped-free support condition. Here, the tube has length $L = 15$ nm and outer diameter $D_o = 2.5$ nm. In this case, the frequencies are certainly lower, as expected with the less strict support condition. We also note that non-coaxial mode shapes are revealed, together with modes for which the inner layers exhibit different shapes from the outer ones. These are not analytically described because they are not basics modes of vibration.

The nature of the support condition remains unclear in the context of CNT applications. When the support is clamped, all degrees of freedom (d.o.f.) of the supported nodes are fixed. However, the tube will be supported in an elastic medium, which may exhibit a stiffness that is smaller than that of the tubes. Consequently, the support will be more elastic and not fixed. In order to examine how the vibrational frequencies are impacted by an elastic support condition, we introduce additional two-node elements. These have zero initial length, i.e., the two nodes are coincident. The stiffness matrix of these elements is as follows:

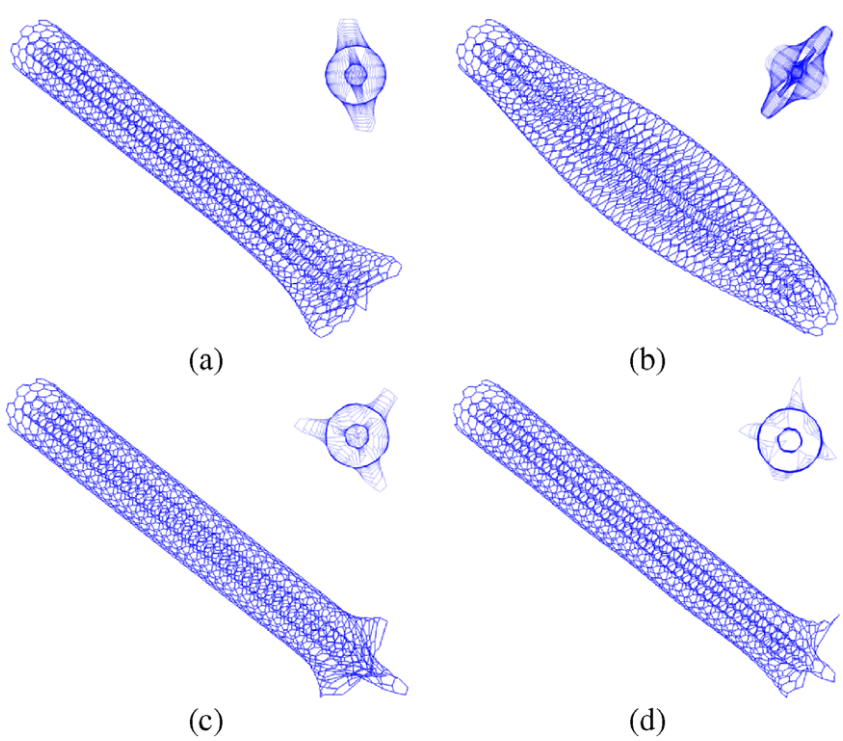

Fig. 5. Breathing modes of vibration of clamped-free supported MWCNTs: (a) first radial, (b) second radial, (c) first triangular, and (d) first cross modes.

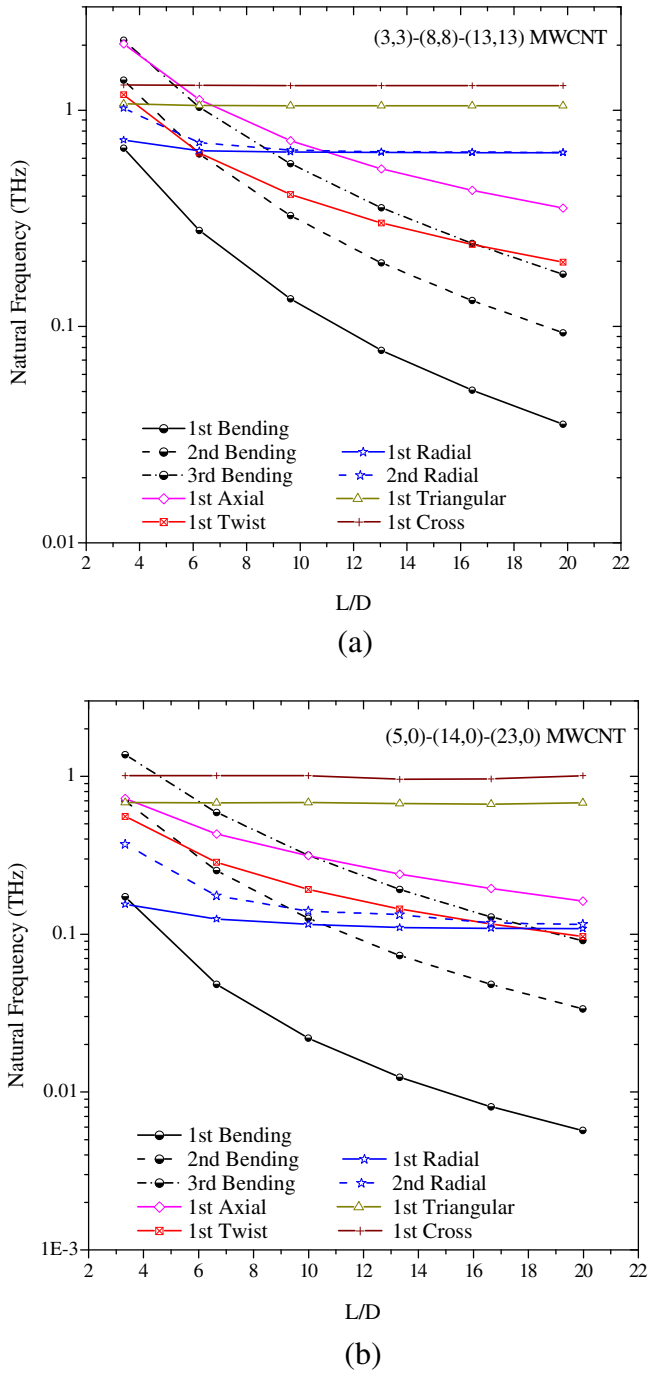

Fig. 6. Natural frequencies vs. aspect ratio of (a) a clamped–clamped supported armchair (3,3)-(8,8)-(13,13) CNT, and (b) a clamped-free supported zigzag (5,0)-(14,0)-(23,0) CNT.

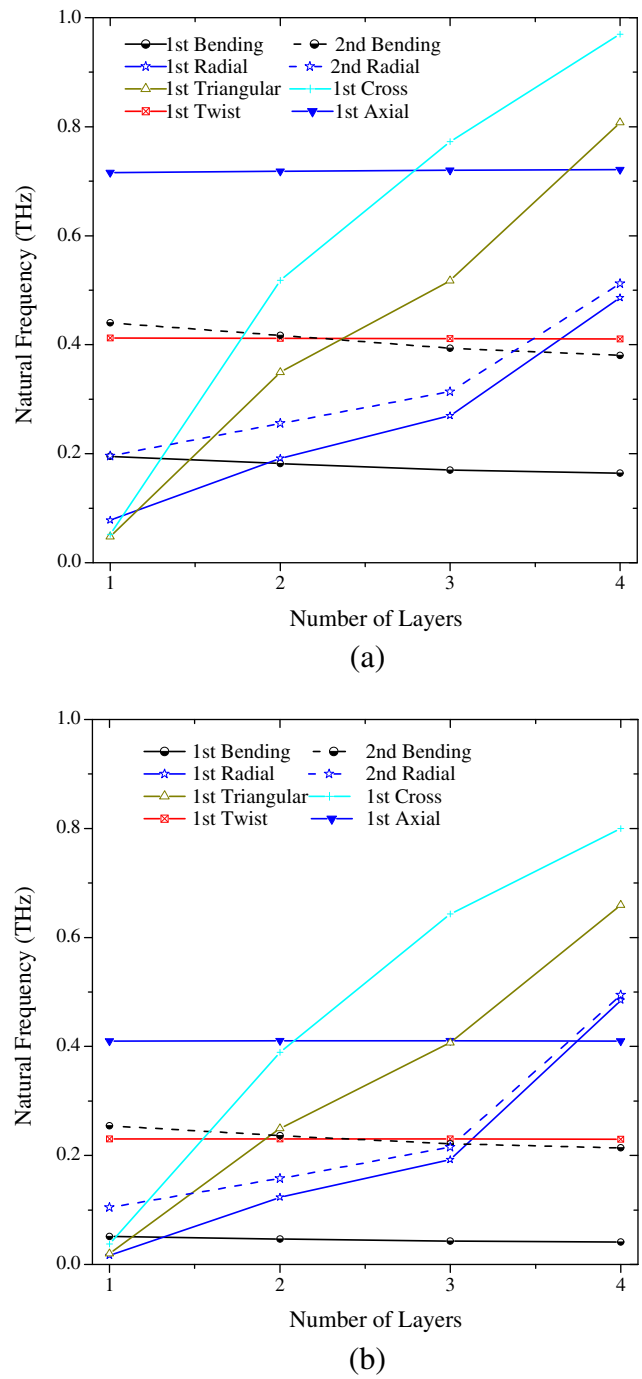

Fig. 7. Natural frequencies of (a) a clamped–clamped armchair CNT with $D_o = 2.45$ nm and $L = 17$ nm, and (b) a clamped-free zigzag CNT with $D_o = 2.5$ nm and $L = 15$ nm with a different number of layers.

$$\begin{bmatrix} k & 0 & 0 & 0 & 0 & 0 & 0 & -k & 0 & 0 & 0 & 0 & 0 \\ & k & 0 & 0 & 0 & 0 & 0 & 0 & -k & 0 & 0 & 0 & 0 \\ & & k & 0 & 0 & 0 & 0 & 0 & 0 & -k & 0 & 0 & 0 \\ & & & k_\theta & 0 & 0 & 0 & 0 & 0 & 0 & -k_\theta & 0 & 0 \\ & & & & k_\theta & 0 & 0 & 0 & 0 & 0 & 0 & -k_\theta & 0 \\ & & & & & k_\theta & 0 & 0 & 0 & 0 & 0 & 0 & -k_\theta \\ & & & & & & k & 0 & 0 & 0 & 0 & 0 & 0 \\ & & & & & & & k & 0 & 0 & 0 & 0 & 0 \\ & & & \text{Symmetric} & & & & & k & 0 & 0 & 0 & 0 \\ & & & & & & & & & k_\theta & 0 & 0 & 0 \\ & & & & & & & & & & k_\theta & 0 & 0 \\ & & & & & & & & & & & k_\theta & 0 \\ & & & & & & & & & & & & k_\theta \end{bmatrix}. \tag{22}$$

The element has six d.o.f. per node, i.e., three translational and three rotational, where k is the stiffness at every translational d.o.f. The rotational d.o.f. have stiffnesses equal to the bond angle bending resistance force constant. The stiffness k takes on various values that are multiples of the carbon–carbon bond stretching constant, which is the major atomic nanotube interaction and is the stiffest observed bond interaction in nature. These elements are positioned at the supported nanotube end. The first node is fixed, while the second is the node that simulates a single atom of the tube end. Hence, the support condition for the nanotube is elastic, with a stiffness equal to that of the above element. Fig. 8 illustrates how the

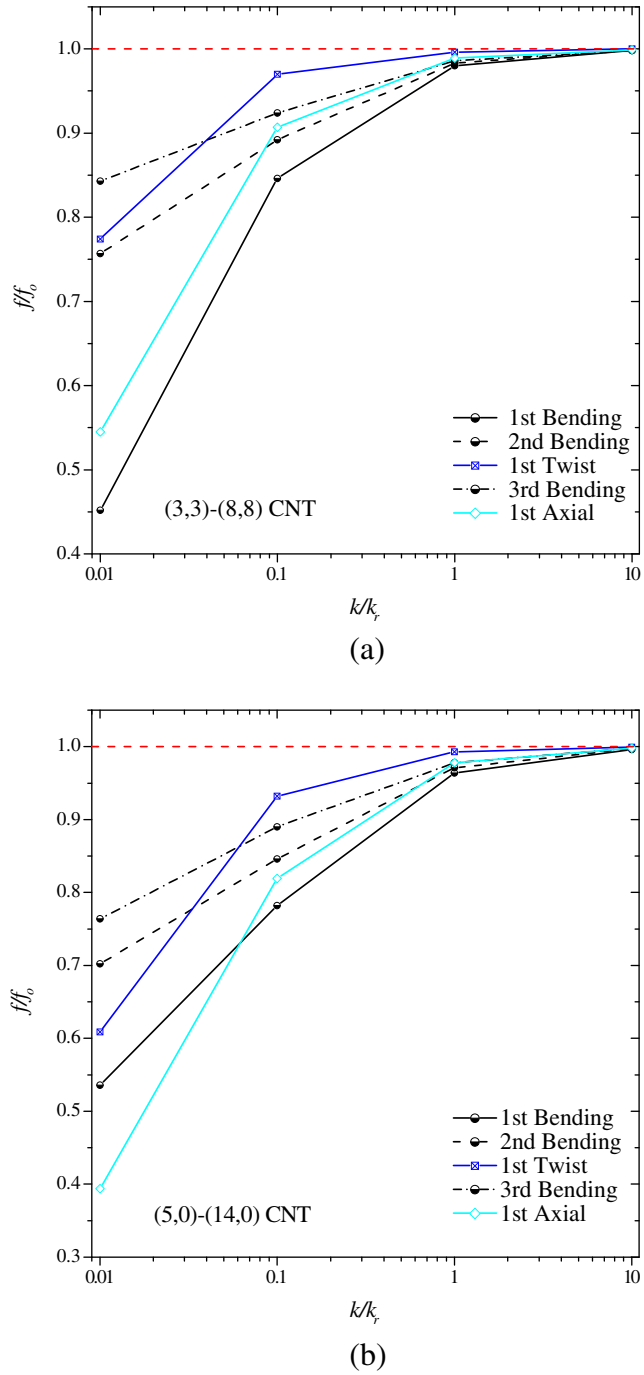

Fig. 8. The effect of elastic support conditions on vibration frequencies for (a) an armchair (3,3)-(8,8) CNT with length $L = 15$ nm supported at both ends, and (b) a zigzag (5,0)-(14,0) CNT supported at one end.

dimensionless frequency f/f_0 for each of the basic modes may be influenced with respect to the stiffness of the elastic support condition. f is the frequency obtained from the eigenvalue analysis of the elastically supported tube and f_0 is the frequency of the corresponding mode obtained from the analysis of the same clamped supported nanotube. Fig. 8a and b depict the behavior of an armchair nanotube with both ends elastically supported and the behavior of a zigzag nanotube with only one end elastically supported. We note a real decrease in the frequencies as the support becomes more elastic. If the stiffness of the rotational d.o.f. changes, there is no remarkable difference in the frequencies.

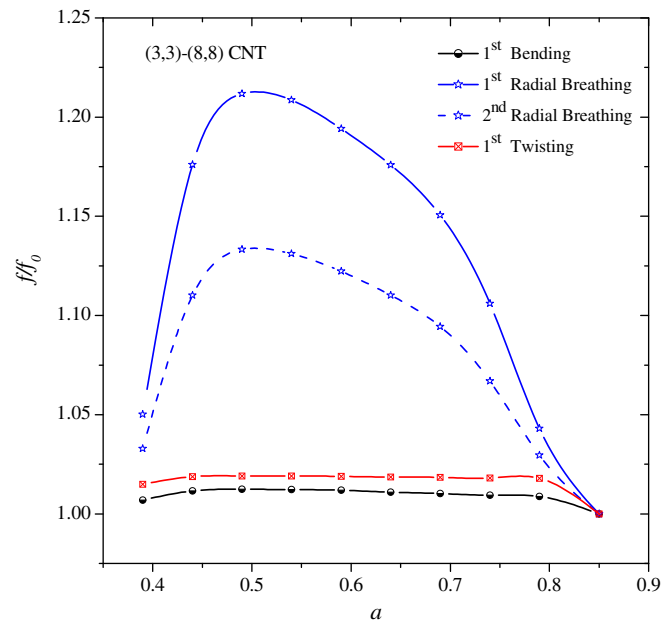

Fig. 9. The effect of van der Waals interactions on the natural frequencies of a clamped–clamped supported (3,3)-(8,8) double-walled CNT.

Finally, we investigate the influence of the van der Waals elements on the vibration behavior of multi-walled nanotubes. In Fig. 9, part of the van der Waals elements are taken into consideration by eliminating those elements that have length greater than a distance a. We then calculate the natural frequencies f. f_0 is the corresponding frequency that results when all of the van der Waals elements are included in the model. The studied nanotube is a (3,3-8,8) CNT of length $L = 11$ nm. We note that our calculations overestimate the frequency f for all mode shapes. The breathing modes are influenced mainly when the discrepancy exceeds 20%. This observation suggests that the van der Waals interactions must be fully included in any model that is used for vibration analysis of MWCNTs. Specifically, it should not be omitted in order to achieve better computational efficiency.

5. Conclusions

In this paper, a linear spring-based model with lumped masses was developed to evaluate the vibrational characteristics of MWCNTs. Specifically, nanosprings were used to simulate the dynamic behavior of the nanotube layers, and van der Waals nanosprings were developed to model the interlayer interactions. The mode shapes and natural frequencies were obtained by solving the eigenvalue problem. Our results suggest additional basic mode shapes for MWCNTs (for example, triangular or cross mode shapes), in addition to the usual mode shapes reported elsewhere. The aspect ratio and number-of-layers were observed to play an important role, significantly influencing the basic modes of vibration of the nanotubes. We examined the effects on the computed frequencies and mode shapes of different constraints at the nanotube ends. We demonstrated the remarkable effect (in terms of decreased natural frequencies) of elastic support conditions on the vibrational frequencies of MWCNTs. We investigated the influence of van der Waals interactions and concluded that the presence of all corresponding elements is necessary in the vibration analysis of MWCNTs. This is particularly true for investigations that explore the relevant breathing modes.

References

[1] R.S. Ruoff, D. Qian, W.K. Liu, C.R. Physique 4 (2003) 993–1008.
[2] M.S. Dresselhaus, G. Dresselhaus, J.C. Charlier, E. Hernandez, Philosophical Transactions of the Royal Society A: Mathematical Physical and Engineering Sciences 362 (2004) 2065–2098.
[3] R.F. Gibson, E.O. Ayorinde, Y. Weng, Composites Science and Technology 67 (2007) 1–28.
[4] D. Garcia-Sanchez, A. San Paulo, M.J. Esplandiu, F. Perez-Murano, L. Forro, A. Aguasca, A. Bachtold, Physical Review Letters 99 (2007) 085501.
[5] B. Liu, Y. Huand, H. Jiang, S. Qu, K.C. Hwang, Computer Methods in Applied Mechanics and Engineering 193 (2004) 1849–1864.
[6] M. Mir, A. Hosseini, G.H. Majzoobi, Computational Materials Science 43 (2008) 540–548.
[7] C. Li, T.-W. Chou, Applied Physics Letters 84 (2004) 121–123.
[8] S.K. Georgantzinos, G.I. Giannopoulos, N.K. Anifantis, Computational Mechanics 43 (2009) 731–741.
[9] Y.W. Kwon, C. Mathena, J.J. Oh, D. Srivastava, Journal of Nanoscience and Nanotechnology 5 (2005) 703–712.
[10] C.M. Wang, V.B.C. Tan, Y.Y. Zhang, Journal of Sound and Vibration 294 (2006) 1060–1072.
[11] J. Yoon, C.Q. Ru, A. Mioduchowski, Journal of Applied Mechanics, Transactions ASME 72 (2005) 10–17.
[12] K.Y. Xu, X.N. Guo, C.Q. Ru, Journal of Applied Physics 99 (2006) 064303.
[13] T. Natsuki, Q.Q. Ni, M. Endo, Carbon 46 (2008) 1570–1573.
[14] K.-Y. Xu, E.C. Aifantis, Y.-H. Yan, Journal of Applied Mechanics, Transactions ASME 75 (2008) 0210131–0210139.
[15] G.I. Giannopoulos, P.A. Kakavas, N.K. Anifantis, Computational Materials Science 41 (2008) 561–569.
[16] S. Iijima, Nature 354 (1991) 56–58.
[17] M.S. Dresselhaus, G. Dresselhaus, R. Saito, Carbon 33 (1995) 883–891.
[18] J. Kołoczek, K. Young-Kyun, A. Burian, Journal of Alloys and Compounds 28 (2001) 222–225.
[19] B.R. Gelin, Molecular Modeling of Polymer Structures and Properties, Hanser/Gardner Publishers, Cincinnati, 1994.
[20] W.D. Cornell, P. Cieplak, C.I. Bayly, I.R. Gould, K.M. Merz Jr., D.M. Ferguson, D.C. Spellmeyer, T. Fox, J.W. Caldwell, P.A. Kollman, Journal of American Chemical Society 117 (1995) 5179–5197.
[21] W.L. Jorgensen, D.L. Severance, Journal of American Chemical Society 112 (1990) 4768–4774.